analytical chemistry

pubs.acs.org/ac Article

Ultrasensitive and Reliable Organic Field-Effect Transistor-Based Biosensors in Early Liver Cancer Diagnosis

Chenfang Sun, Rui Li, Yaru Song, Xiaoqian Jiang, Congcong Zhang, Shanshan Cheng,* and Wenping Hu

Cite This: *Anal. Chem.* 2021, 93, 6188−6194 Read Online

ACCESS | Metrics & More | Article Recommendations | Supporting Information

ABSTRACT: Organic field-effect transistors (OFETs) are considered as one of the cost-effective biosensor devices with rapid detection capabilities and multiparameter responses. However, the functionalization processes on normal organic devices might impact the device performance for its further sensitive and reliable sensing applications. Herein, we develop a novel organic material, 2,6-bis(4-formylphenyl)-anthracene (BFPA) for use as the protective and functional layer of OFET-based biosensors, enabling ultrasensitive determination of alpha-fetoprotein (AFP) with femtomolar accuracy in human serum. By monitoring changes of the source−drain current (I_{ds}) and threshold voltage (V_{th}) electrical signals, the device exhibits improved reliability in detecting AFP biomarkers and is able to differentiate between liver cancer patients and healthy individuals. Featuring label-free determination, shorter analysis time, and lower sample volume, this ultrasensitive and reliable OFET-based biosensor displays numerous advantages over traditional strategies such as enzyme-linked immunosorbent assay and electrochemiluminescence immunoassay, demonstrating that the proposed OFET-based biosensors have broader analytical and clinical applications for early liver cancer diagnosis.

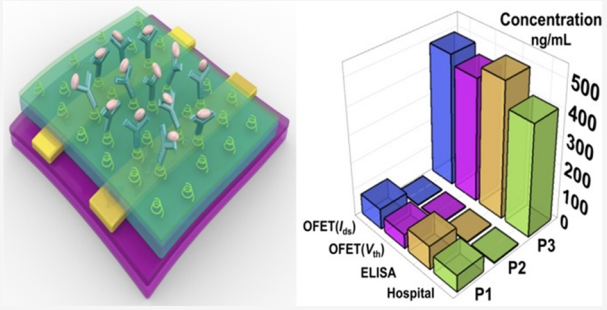

INTRODUCTION

Organic field-effect transistor (OFET)-based sensors[1−6] are considered as advanced biosensing platforms due to their inherent capability for multiparameter accessibility, facile fabrication, rapid detection, and potentially low-cost application to solution processing. Specifically, OFETs show great technological potential for sensing biochemical molecules,[7,8] monitoring cell activity,[9] and tracking drug activity[10] in health treatments. Moreover, OFET-based biosensors can be integrated into large-scale manufacturing using flexible and high temporal resolution arrays for health monitoring appliances.[11,12] Nevertheless, such biosensors have major limitations: for example, the performance of most organic semiconductors (OSCs) degrades rapidly when exposed to moisture.[13] Therefore, the choice of suitable OSC materials[14−16] is of great importance for improving the performance of OFET-based biosensors. Polymer OSCs, especially DPP-based π-conjugated polymer OSCs,[17−21] exhibit excellent shelf-life under ambient conditions through the rational design of their backbone structures and alkyl side chains. The main advantages of DPP-based π-conjugated polymer OSCs are their mechanical flexibility and large-area preparation through simple solution-processing methods, e.g., spin-coating, ink-jet, or silk-screen printing. In addition, the alkyl chain exposed to the surface of the polymer is hydrophobic, which protects the carrier transport in a solvent environment. For instance, polymer-based OFET devices have been shown to resist degradation for more than 1 week and may retain their original electrical performance over a prolonged period in the presence of a protecting gel layer.[22] Nonetheless, challenges such as the introduction of functional groups on normal organic devices remain to be addressed for further sensitive and reliable sensing applications. Recently, two typical approaches to OSC functionalization have been considered, offering more efficient ways to bind specific receptors for sensitive OFET-based biosensors. The most common strategy involves synthesis processes. Miao and co-workers[23] tailored a variety of functional groups onto OSCs, which provided a general sensing platform for highly sensitive and selective detection of streptavidin. A second strategy depends on chemical modifications to introduce functional groups such as aldehyde,[24] amino,[25] and carboxyl goups[26,27] on OSCs to create a bridge for the immobilization of biological receptors through bioconjugation chemistry. Zhu and co-workers[27] introduced a molecular antenna onto organic devices using a plasma-assisted interfacial-grafting technique. This specific interaction results in determination of adenosine triphosphate with excellent selectivity, good reproducibility, and low

Received: January 26, 2021
Accepted: March 19, 2021
Published: March 29, 2021

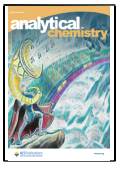

https://doi.org/10.1021/acs.analchem.1c00372
Anal. Chem. 2021, 93, 6188−6194

detection limits. However, complicated synthesis and chemical functionalization processes lead to an unpredictable decrease in OFET performance. In addition, although such single-signal sensing strategies have demonstrated good results in clinical diagnosis, there is a strong desire to develop more reliable OFET-based biosensors with multiparameter responses, e.g., source−drain current (I_{ds}) and threshold voltage (V_{th}) electrical signals for further biomedical applications.

In this work, we report the development of an ultrasensitive and reliable OFET-based biosensor modified with 2,6-bis(4-formylphenyl)anthracene (BFPA) materials and its application to determine the concentration of AFP biomarkers in clinical early liver cancer diagnosis. BFPA materials are used to maintain device performance as the protective layer and efficiently immobilize antibody receptors as the functional layer. Our results demonstrate that the limit of detection can reach as low as femtomolar (fM) levels through monitoring the changes of I_{ds} and V_{th} electrical signals. Featuring short analytical time, less sample volume, and high accuracy, the proposed ultrasensitive and reliable label-free OFET-based biosensor exhibits competitive detection abilities with traditional methods such as the enzyme-linked immunosorbent assay (ELISA) and electrochemiluminescence (ECL) immunoassay, thereby providing a new detection platform for liver cancer.

EXPERIMENTAL SECTIONS

Chemicals and Materials. 2,6-Dibromoanthracene, 4-(4,4,5,5-tetramethyl-1,3,2-dioxaborolan-2-yl)benzaldehyde, and tetrakis(triphenylphosphine)palladium were purchased from Bide pharmatech Co., Ltd., Tianjin, China. The alpha-fetoprotein (AFP) ELISA kit was purchased from Wuhan Youersheng Trading Co., Ltd., Hubei, China. Ethanolamine (EA) was purchased from 3A Chemicals Co., Ltd., Tianjin, China. Human serum albumin (HSA), AFP antigens, and AFP antibodies were purchased from MyBioSource Inc., Vancouver, USA. Fluorescein-labeled AFP antibodies were obtained from Abcam Co., Ltd., Tianjin, China. Phosphate buffer solution (1 × PBS, pH = 7) was prepared in the lab using 137.00 mM NaCl, 8.10 mM $Na_2HPO_4{\cdot}12H_2O$, 2.70 mM KCl, and 1.50 mM KH_2PO_4.

Apparatus. Nuclear magnetic resonance (NMR) spectra were recorded using a Bruker ADVANCE 400 NMR spectrometer. An AEI-MS50-MS spectrometer was used for molecular weight determination. The number-average molar mass (M_n) and dispersity ($Đ$) of the PDVT-8 polymer were measured using PL-GPC220 gel permeation chromatography. Confocal laser scanning microscopy (CLSM) images were obtained using a Zeiss LSM 800. Atomic force microscopy (AFM) images were captured in tapping mode in air using a Bruker Dimension Icon. X-ray photoelectron spectroscopy (XPS) measurement was performed using an Axis Ultra DLD (Kratos, UK) ultrahigh vacuum photoelectron spectroscope with Al Kα radiation (1486.6 eV). The optical density in ELISA kit test was measured at 450 nm.

Fabrication of BFPA-Modified OFETs. The PDVT-8 polymer was prepared via Stille coupling polymerization[18] in Figure S1, and BFPA was synthesized by the Pd-catalyzed Suzuki coupling reaction[28] in Figure S2. Full details of these processes are provided in the Supporting Information. The fabrication process of the OFET-based biosensor is illustrated in Figure 1a. The heavily n-doped SiO_2/Si substrate was first cleaned with deionized water, piranha solution, and isopropyl alcohol and treated with oxygen plasma. Subsequently, the as-obtained substrate was modified with octadecyltrichlorosilane (OTS) by conventional vapor deposition[29] at 120 °C for 2 h, and extra OTS was removed using hexane, trichloromethane, and isopropanol. Thereafter, 30 nm gold source (S) and drain (D) electrodes were deposited on the substrate. Afterward, the PDVT-8 solution (5 mg/mL in chlorobenzene) was spin-coated and then annealed on a hotplate to enhance the morphology and firmness of the polymer film. Finally, a thin protective and functional BFPA layer was modified on the device to maintain its performance in Figure S3 and guarantee efficient immobilization of AFP antibodies as receptors in Figure 2.

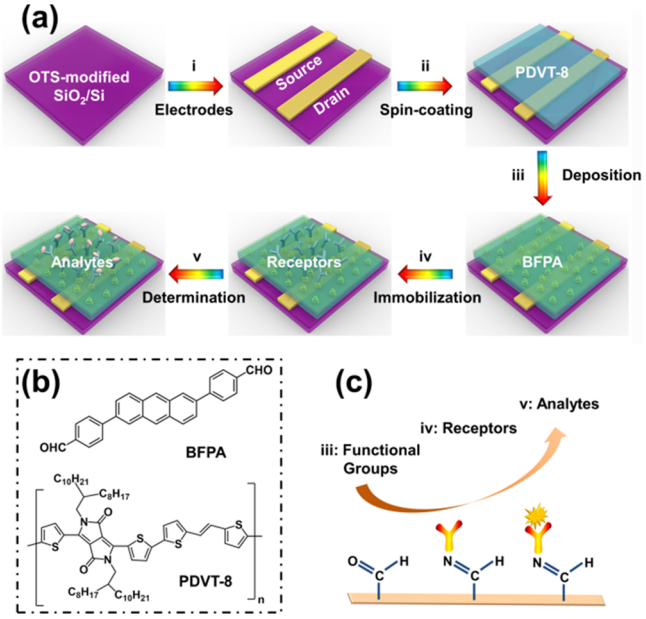

Figure 1. Schematic representation of the bottom-gate and bottom-contact OFET-based biosensors. (a) Fabrication of OFET-based biosensors. (i) Au source and drain electrodes are deposited on OTS-modified SiO_2/Si substrates; (ii) PDVT-8 film is spin-coated as the charge transport layer; (iii) BFPA functional layer is modified on the device as the functional layer; (iv, v) AFP antibodies are immobilized to form the receptor layer for the determination of target AFP biomarkers. (b) Chemical structure of the organic molecules (BFPA and PDVT-8). Their synthetic routes are shown in Figures S1 and S2. (c) Schematics showing surface modification (iii) to immobilize antibodies as receptors (iv) for the determination of target AFP biomarkers (v).

Determination of AFP Biomarkers in Human Serum. Human serum is an ideal sample for biological and medical applications because it provides considerable information about various disease hints released from the human bodies. First, we followed a standard operating procedure for real-sample pretreatment.[30] To determine AFP biomarkers in human serum, EA-capped OFETs were measured at least five times to ensure stable electrical signals. Thereafter, pretreated serum samples from three volunteers were evaluated by the proposed OFET-based biosensors. The obtained results were consistent with both the commercial ELISA kit and ECL immunoassay in early liver cancer diagnosis, demonstrating that the proposed OFET-based biosensors have potential applications for point-of-care diagnosis.

https://doi.org/10.1021/acs.analchem.1c00372
Anal. Chem. 2021, 93, 6188−6194

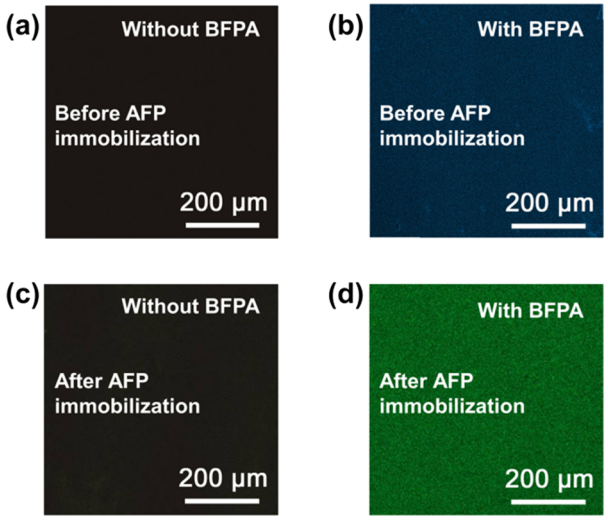

Figure 2. Morphological characteristics of the BFPA functional layer by CLSM. (a) Typical CLSM image exhibiting dark fluorescence without the BFPA functional layer before antibody immobilization. (b) Typical CLSM image exhibiting blue fluorescence with the BFPA functional layer before antibody immobilization. (c) Typical CLSM image exhibiting dark fluorescence without the BFPA functional layer after antibody immobilization. (d) Typical CLSM image exhibiting green fluorescence with the BFPA functional layer after antibody immobilization.

RESULTS AND DISCUSSION

The integration of the OFET device and functional layer in the fabrication of OFET-based biosensors plays a leading role in analytical chemistry. The resulting nontoxic functional layer[1,31−33] exhibits several desirable benefits such as (i) facile and convenient modification, (ii) stable and quick responses, (iii) high specific surface area, (iv) excellent universality with a wide range of recognition elements, and (v) possibilities of surface reset via a simple polishing step. Herein, a novel material, BFPA, was synthesized for the protective and functional layer required to maintain device performance as well as efficient receptor immobilization for biological applications. The devices were achieved simply according to the following process: (i) Au source and drain electrodes are deposited on OTS-modified SiO_2/Si substrates; (ii) PDVT-8 film is spin-coated as the charge transport layer; (iii) the BFPA functional layer is modified on the device, providing a moderate distribution of aldehyde groups for antibodies immobilization; (iv, v) AFP antibodies are immobilized to form the receptor layer and then capped with 10 nM EA to reduce nonspecific adsorption. The efficiency of the prepared materials was measured by monitoring changes of I_{ds} and V_{th} electrical signals after the incubation of the target AFP biomarkers. Device fabrication, structural formulas of the materials, and binding mechanism are illustrated in Figure 1.

Morphological Studies of the BFPA Functional Layer. Prior to electrochemical studies, confocal laser scanning microscopy (CLSM) was employed to characterize the BFPA functional layer. As shown in Figure 2, the immobilization properties of AFP antibodies are significantly improved through the modification of the BFPA material. For instance, the unmodified PDVT-8 film exhibits dark fluorescence in Figure 2a, whereas that shown in Figure 2b exhibits the expected blue fluorescent light (Figure S4), denoting complete surface functionalization of the BFPA functional layer. Fluorescein-labeled AFP antibodies were also used to confirm the successful antibody immobilization on the surface of the BFPA functional layer. The unmodified film exhibits dark fluorescence in Figure 2c, whereas in Figure 2d, the PDVT-8 film exhibits the expected green fluorescent light due to antibody immobilization. Therefore, the large-area modification of the BFPA functional layer has the potential for further efficient immobilization of antibodies as receptors.

Electrochemical Characterization of BFPA-Modified OFETs. The electrical characteristics of BFPA-modified OFETs were tested using a Keithley 4200SCS. To improve the quality of the PDVT-8 film, there is an annealing surface treatment process (170 °C, 10 min) before deposition of the BFPA functional layer. The operational mechanism of the device can be explained as follows: when a gate voltage is applied, carriers are induced at the interface between the PDVT-8 layer and the SiO_2 dielectric layer, forming a conductive channel. The carriers are then driven from the source electrode to the drain electrode under the source−drain voltage. In our experiments, the transfer characteristics of the saturation regime were measured by sweeping the gate voltage (V_g) between 10 and −60 V while maintaining a constant drain voltage constant of −60 V. The observed transfer curves shown indicated that the number of carriers could be controlled by an externally applied V_g in Figure 3, resulting in gate-tunable

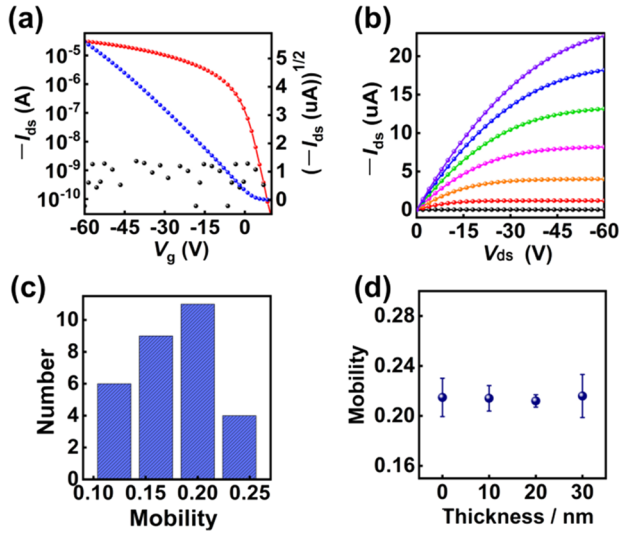

Figure 3. Electrochemical characteristics of BFPA-modified OFETs. (a) Transfer characteristics of BFPA-modified OFETs. The black dots denote I_{gs}. (b) Output characteristics of BFPA-modified OFETs. V_g ranges from 0 to −60 V with a step of −10 V. (c) Spatial distribution of mobility in the saturation regime. (d) Influence of BFPA thicknesses on the performance of the OFET devices. All the measurements are performed 10 times, and the data points are the average over the three replicates, while error bars are the relevant standard deviations.

charge transport characteristics. Black dots indicate the leakage current (I_{gs}). Further characterization was achieved by measuring the output curve in Figure 3b by sweeping V_g from 0 to −60 V with a step of −10 V, resulting in a clear transition from a linear regime to a saturation regime. The average carrier mobility was 0.18 $cm^2 V^{-1} s^{-1}$, with a maximum hole mobility of 0.24 $cm^2 V^{-1} s^{-1}$, as shown in Figure 3c. This may be expressed as $I_{ds} = W\mu C_i(V_g - V_{th})^2/2L$, where C_i = 10 nF cm^{-2} was employed in all mobility calculations.[34]

https://doi.org/10.1021/acs.analchem.1c00372
Anal. Chem. 2021, 93, 6188−6194

Additionally, we investigated the impact of the BFPA functional layer on device performance (Figure 3d), the results of which show that mobility remains stable under various thicknesses of the BFPA functional layer, denoting limited degradation of device performance (Figure S3). Considering the optimization results, a thickness of 20 nm BFPA functional layer was chosen to modify the device with smaller standard deviations. The observed nondestructive phenomenon on device performance can be explained as follows: the PDVT-8 material serves as the charge transport layer while the BFPA material serves as the protective and functional layer. It has been confirmed that the effective thickness of the PDVT-8 conducting channel is approximately 4 nm.[18] Herein, the optimized film thickness of the PDVT-8 channel layer was found to be 25.01 nm (Figure S5), i.e., considerably greater than 4 nm. This result indicates that the thickness of the BFPA functional layer does not influence charge transportation. Furthermore, the stability of the OFET-based biosensor was tested under 20 measurements in Figure S6 with excellent reproducibility, indicating that the uniform and ordered PDVT-8 polymer film could maintain stable operation in the aqueous phase with the proposed BFPA material used as the protective and functional layer.

Immobilization of Antibodies as Receptors on the BFPA Functional Layer. To convert BFPA-modified OFETs into biosensors, antibodies specific to AFP biomarkers are first immobilized on the BFPA functional layer as receptors. All measurements were performed after enough rinsing with 0.01× PBS (phosphate-buffered solution, pH = 7) to improve the reproducibility of sensors. The immobilization process was optimized using atomic force microscopy (AFM) to determine the attachment and coverage of AFP antibodies. OFETs functionalized with AFP antibodies were incubated for 1 h with a concentration of 50 μg/mL. Afterward, the chips were rinsed with 0.01× PBS to remove excess antibodies followed by DI to clean the salts from the OFET surface and finally dried with argon for AFM characterization. Figure 4 confirms the immobilization of the AFP antibodies on the BFPA functional layer. The changes of thickness were measured at several different locations while a single step was shown as a representative plot. The relative height increased from 44.21 to 49.74 nm after the immobilization of the AFP antibodies in Figure 4a,b, which was consistent with earlier reports.[24] In addition, the surface roughness of the antibody-conjugated film also increased from 3.99 to 4.30 nm in Figure 4c,d, suggesting the effective immobilization.[35] Moreover, successful antibody immobilization was further affirmed by XPS measurements. Before antibody immobilization, no detectable nitrogen (N 1s) signal was present (Figure S7, black line). After immobilization, the signal was greatly enhanced (Figure S7, red line) as a result of the presence of nitrogen-rich proteins. Combined, these pieces of evidence suggest the successful immobilization of AFP antibodies.

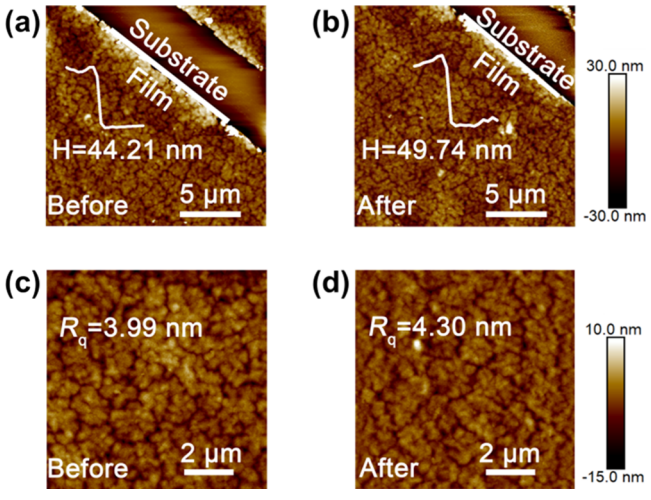

Figure 4. Morphological characteristics of the antibody immobilization by AFM. (a) Typical AFM image showing the height of 44.21 nm before antibody immobilization. (b) Typical AFM image showing the height of 49.74 nm after antibody immobilization. (c) Typical AFM image exhibiting a root mean square roughness of 3.99 nm before antibody immobilization. (d) Typical AFM image exhibiting a root mean square roughness of 4.30 nm after antibody immobilization.

Electrical Responses to Target AFP Biomarkers. Hepatocellular carcinoma is a tumor disease characterized by acute onset, high incidence, and high mortality rate.[36] Overexpressed AFP biomarkers act widely as indicators of this disease.[37] Thus, the determination of these biomarkers is crucial for clinical early liver cancer diagnosis.[38] By virtue of the efficient immobilization with the protective and functional BFPA layer as well as unique properties of OFETs with multiparameter electrical signals, we have designed an ultrasensitive and reliable OFET-based biosensor for early liver cancer diagnosis. The output electrical signals are affected by biochemical reactions between antibodies and antigens before transduction and then amplified by this OFET-based biosensor. In the present work, determination was achieved by monitoring changes of I_{ds} and V_{th} electrical signals after AFP biomarker incubation. The response may be evaluated directly as follows: $\triangle I_{ds} = (I - I_0)/I_0$ and $\triangle V_{th} = V - V_0$, where I and V are the electrical signals measured after AFP biomarkers incubation, and I_0 and V_0 are the electrical signals measured before AFP biomarkers incubation. To reduce nonspecific binding events, antibody-immobilized OFETs were capped with 10 nM EA prior to the incubation of target samples. Our results demonstrate decreased I_{ds} (32.08%) and negatively shifted V_{th} (3.72 V) after a 1 μg/mL AFP antigen solution was incubated in the sensing region. In the controlled device, both the I_{ds} and V_{th} electrical signals are negligible in 1 μg/mL HSA, confirming that I_{ds} and V_{th} electrical signals contribute to specific anti-AFP/AFP binding events (Figure 5a,b). For further quantitative detection, this OFET-based biosensor was investigated by monitoring I_{ds} and V_{th} electrical signals of various concentrations of AFP biomarkers, ranging from 10 pg/mL to 1 μg/mL. The responses indicate limits of detection of 45 fM for I_{ds} as the sensing signal and 53 fM for V_{th} as the sensing signal in Figure 5c,d. Their sensitivity is also greatly enhanced relative to our previously reported biosensors[39] as a result of the introduction of the protective and functional BFPA layer. This indicates that the prepared OFET-based biosensors have promise as clinical detectors within the detection limit lower than the cut-off value.[40] Furthermore, having multiparameter electrical signals, the BFPA functional layer[41] exhibits excellent reliability for monitoring target AFP biomarkers in complex human serum samples, as well as for differentiating liver cancer patients from healthy individuals.

Mechanism of the OFET-Based Biosensor. Electrical output responses are strongly dependent on protein charges at different pH values. Specifically, the isoelectric point (pI) of the AFP biomarker occurs at 4.9. At pH values greater than the

https://doi.org/10.1021/acs.analchem.1c00372
Anal. Chem. 2021, 93, 6188−6194

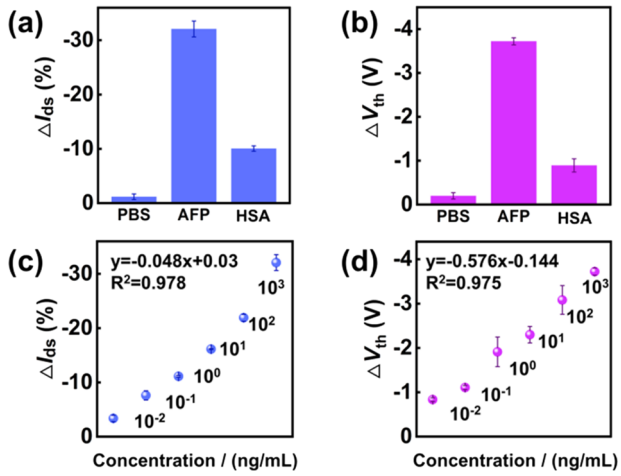

Figure 5. Electrical responses of the proposed OFET-based biosensors. (a) Sensing behavior of the I_{ds} electrical signal in response to various analytes (1× PBS, 1 μg/mL AFP, and 1 μg/mL HSA). (b) Sensing behavior of the V_{th} electrical signal in response to various analytes (1× PBS, 1 μg/mL AFP, and 1 μg/mL HSA). (c) Linear fitting curve of the I_{ds} electrical signal at different concentrations of AFP biomarkers. (d) Linear fitting curve of the V_{th} electrical signal at different concentrations of AFP biomarkers. All the measurements are performed 10 times, and the data points are the average over the three replicates, while error bars are the relevant standard deviations.

pI, there is a high density of COO^- in the anti-AFP/AFP complex (Figure 6a), resulting in weak electrostatic inter-

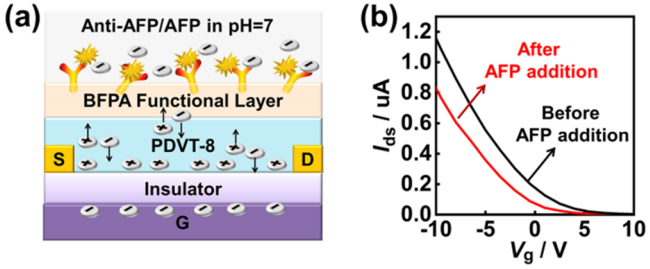

Figure 6. Schematic mechanism of OFET-based biosensors. (a) Model for immune detection when the target AFP biomarker is diluted in 1× PBS at pH = 7. (b) Changes of I_{ds} and V_{th} electrical signals in response to 1 μg/mL AFP biomarkers.

actions between the channel region and surface charges. Therefore, there is a notable decrease in the I_{ds} electrical signal and a negative shift in the V_{th} electrical signal compared with the baseline (black line) following the reaction with target AFP biomarkers (red line) in Figure 6b. This decrease in I_{ds} can be attributed to depleted holes in the channel region resulting from higher levels of negative charges acting as channel traps; this makes the device harder to turn on, causing V_{th} shifts to a negative direction. It is well-known that charge screening effects occur when detecting charges exceed the Debye length (λ_D).[42] In this work, AFP antigen and antibody interactions require salts to maintain bond stability; therefore, significant charge screening effects might occur at short λ_D = 0.7 nm in 1× PBS.[43] To further guarantee the effective detection, the *Donnan* effect is proposed,[44] in which proteins are considered as a charged molecule layer on the device and small ions can shuffle between the 1× PBS and proteins. Following the incubation of biomarkers, the redistribution of ions at the interface creates a detectable change in the interfacial potential. Therefore, biomolecules could then be detected via surface-charge sensing devices, such as OFETs.

Clinical Applications in Human Serum. Taking into consideration the above mechanism, further investigations were performed in order to demonstrate the applicability and reliability of OFET-based biosensors. The AFP ELISA kit test is a widely used strategy to screen men with high AFP levels in early liver cancer diagnosis. Typically, the ELISA kit requires two kinds of antibodies that recognize separate epitopes on the target antigen and bind simultaneously to the biomolecule. Nevertheless, the label-based ELISA method relies on long-time experimental procedures, hindering early cancer diagnosis. Hence, the rapid detection of biomarkers in human serum based on label-free OFET-based biosensor is especially important for clinical applications. Herein, pretreated samples collected from three volunteers were first measured by commercial AFP ELISA kits and then analyzed by this proposed OFET-based biosensor. It was shown that the results were both consistent with the commercial AFP ELISA kits as well as with the clinical monitoring values based on the ECL immunoassay (Table S1). Moreover, the concentrations of AFP biomarkers from liver cancer patients were significantly higher than those from healthy individuals in Figure 7,

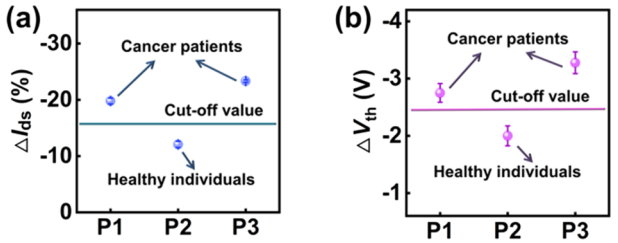

Figure 7. Clinical applications of OFET-based biosensors. (a) Determination of AFP biomarkers in human serum samples with I_{ds} as the sensing signal. (b) Determination of AFP biomarkers in human serum samples with V_{th} as the sensing signal. All the measurements are performed 10 times, and the data points are the average over the three replicates, while error bars are the relevant standard deviations.

indicating that OFET-based biosensors can also distinguish liver cancer patients from healthy individuals. Combined with the above observations, OFET-based biosensors are shown to have remarkable potential for early liver cancer diagnosis. Featuring ultrasensitivity (fM level), a dual-signal response (I_{ds} and V_{th}), shorter analysis time (40 min), and lower sample volume (20 μL), this novel OFET-based biosensor has numerous advantages relative to traditional strategies and is a reliable diagnostic platform for monitoring early liver cancer.

CONCLUSIONS

In summary, combining the inherent electrical signals of OFETs and the intrinsic physicochemical properties of biomarkers, we proposed a novel OFET-based biosensor using BFPA material as the protective and functional layer for ultrasensitive and reliable determination of AFP biomarkers down to the femtomolar level (45 fM for I_{ds} as the sensing signal and 53 fM for V_{th} as the sensing signal) in human serum. Furthermore, thanks to its multi-parameter electrical signals, the device exhibits improved reliability in monitoring target AFP biomarkers in human serum and it can differentiate between liver cancer patients and healthy individuals.

https://doi.org/10.1021/acs.analchem.1c00372
Anal. Chem. 2021, 93, 6188−6194

Featuring label-free determination, shorter analysis time (40 min), and lower sample volume (20 μL), this proposed OFET-based biosensor displays numerous advantages over traditional strategies such as the ELISA and ECL immunoassay, suggesting that this OFET-based biosensor might serve as a reliable tool in early liver cancer diagnosis.

■ ASSOCIATED CONTENT

Supporting Information

The Supporting Information is available free of charge at https://pubs.acs.org/doi/10.1021/acs.analchem.1c00372.

Synthetic route of the PDVT-8 material and BFPA material and related characteristics for OFET-based biosensors (PDF)

■ AUTHOR INFORMATION

Corresponding Author

Shanshan Cheng − *Department of Chemistry, Tianjin Key Laboratory of Molecular Optoelectronic Sciences, School of Science, Tianjin University, Tianjin 300072, China; Joint School of National University of Singapore and Tianjin University, Fuzhou International Campus, Tianjin University, Fuzhou 350207, China;* orcid.org/0000-0001-7282-2802; Email: chengss@tju.edu.cn

Authors

Chenfang Sun − *Department of Chemistry, Tianjin Key Laboratory of Molecular Optoelectronic Sciences, School of Science, Tianjin University, Tianjin 300072, China*

Rui Li − *Department of Chemistry, Tianjin Key Laboratory of Molecular Optoelectronic Sciences, School of Science, Tianjin University, Tianjin 300072, China*

Yaru Song − *Department of Chemistry, Tianjin Key Laboratory of Molecular Optoelectronic Sciences, School of Science, Tianjin University, Tianjin 300072, China*

Xiaoqian Jiang − *Department of Chemistry, Tianjin Key Laboratory of Molecular Optoelectronic Sciences, School of Science, Tianjin University, Tianjin 300072, China*

Congcong Zhang − *Institute for Advanced Interdisciplinary Research (iAIR), Collaborative Innovation Center of Technology and Equipment for Biological Diagnosis and Therapy in Universities of Shandong, University of Jinan, Jinan 250011, China*

Wenping Hu − *Department of Chemistry, Tianjin Key Laboratory of Molecular Optoelectronic Sciences, School of Science, Tianjin University, Tianjin 300072, China; Beijing National Laboratory for Molecular Science, Key Laboratory of Organic Solids, Institution of Chemistry, Chinese Academy of Sciences, Beijing 100190, China; Joint School of National University of Singapore and Tianjin University, Fuzhou International Campus, Tianjin University, Fuzhou 350207, China;* orcid.org/0000-0001-5686-2740

Complete contact information is available at: https://pubs.acs.org/10.1021/acs.analchem.1c00372

Author Contributions

C.S.: conceptualization, data curation, investigation, methodology, writing of the original draft, and review & editing. R.L.: methodology. Y.S.: review & editing. X.J.: investigation. C.Z.: investigation. S.C.: project administration, supervision, and review & editing. W.H.: project administration, supervision, and review & editing. The manuscript was written through contributions of all authors, and all authors had given approval to the final version of the manuscript.

Notes

The authors declare no competing financial interest.

■ ACKNOWLEDGMENTS

The authors sincerely acknowledged Prof. Xiaotao Zhang for professional discussion on materials design, Prof. Jinhai Huang on ELISA experiments, and Don Li for cover art layout. This work was financially supported by the Ministry of Science and Technology of China (grant nos. 2016YFB0401100, 2017YFA0204503 and 2015CB856502) and the Natural Science Foundation of China (grant nos. 21705116, 51733004, 91433115, 51633006, 51703160, 21661132006, and 21473222).

■ REFERENCES

(1) Wang, N.; Yang, A.; Fu, Y.; Li, Y.; Yan, F. *Acc. Chem. Res.* **2019**, *52*, 277−287.

(2) Zhang, C.; Chen, P.; Hu, W. *Chem. Soc. Rev.* **2015**, *44*, 2087−2107.

(3) Li, H.; Shi, W.; Song, J.; Jang, H. J.; Dailey, J.; Yu, J.; Katz, H. E. *Chem. Rev.* **2019**, *119*, 3−35.

(4) Hu, W.; Liu, Y.; Xu, Y.; Liu, S.; Zhou, S.; Zhu, D. *Synth. Met.* **1999**, *104*, 19−26.

(5) Hu, W.; Liu, Y.; Xu, Y.; Liu, S.; Zhou, S.; Zhu, D.; Xu, B.; Bai, C.; Wang, C. *Thin Solid Films* **2000**, *360*, 256−260.

(6) Fu, Y.; Wang, N.; Yang, A.; Law, H. K.; Li, L.; Yan, F. *Adv. Mater.* **2017**, *29*, 1703787.

(7) Khan, H. U.; Jang, J.; Kim, J. J.; Knoll, W. *J. Am. Chem. Soc.* **2011**, *133*, 2170−2176.

(8) Khan, H. U.; Roberts, M. E.; Johnson, O.; Förch, R.; Knoll, W.; Bao, Z. *Adv. Mater.* **2010**, *22*, 4452−4456.

(9) Kyndiah, A.; Leonardi, F.; Tarantino, C.; Cramer, T.; Millan-Solsona, R.; Garreta, E.; Montserrat, N.; Mas-Torrent, M.; Gomila, G. *Biosens. Bioelectron.* **2020**, *150*, 111844.

(10) Jang, Y.; Jang, M.; Kim, H.; Lee, S. J.; Jin, E.; Koo, J. Y.; Hwang, I. C.; Kim, Y.; Ko, Y. H.; Hwang, I.; Oh, J. H.; Kim, K. *Chem* **2017**, *3*, 641−651.

(11) Lee, W.; Kim, D.; Rivnay, J.; Matsuhisa, N.; Lonjaret, T.; Yokota, T.; Yawo, H.; Sekino, M.; Malliaras, G. G.; Someya, T. *Adv. Mater.* **2016**, *28*, 9722−9728.

(12) Wang, S.; Xu, J.; Wang, W.; Wang, G. J. N.; Rastak, R.; Molina-Lopez, F.; Chung, J. W.; Niu, S.; Feig, V. R.; Lopez, J.; Lei, T.; Kwon, S.-K.; Kim, Y.; Foudeh, A. M.; Ehrlich, A.; Gasperini, A.; Yun, Y.; Murmann, B.; Tok, J. B. H.; Bao, Z. *Nature* **2018**, *555*, 83−88.

(13) Roberts, M. E.; Mannsfeld, S. C. B.; Tang, M. L.; Bao, Z. *Chem. Mater.* **2008**, *20*, 7332−7338.

(14) Li, J.; Li, H.; Xu, L.; Wang, L.; Hu, Z.; Liu, L.; Huang, Y.; Kotov, N. A. *SmartMat* **2021**, e1019.

(15) Yao, Y.; Chen, Y.; Wang, H.; Samorì, P. *SmartMat* **2020**, *1*, e1009.

(16) Zhou, K.; Dai, K.; Liu, C.; Shen, C. *SmartMat* **2020**, *1*, e1010.

(17) Li, J.; Zhao, Y.; Tan, H. S.; Guo, Y.; Di, C. A.; Yu, G.; Liu, Y.; Lin, M.; Lim, S. H.; Zhou, Y.; Su, H.; Ong, B. S. *Sci. Rep.* **2012**, *2*, 754.

(18) Chen, H.; Guo, Y.; Yu, G.; Zhao, Y.; Zhang, J.; Gao, D.; Liu, H.; Liu, Y. *Adv. Mater.* **2012**, *24*, 4618−4622.

(19) Yi, Z.; Jiang, Y.; Xu, L.; Zhong, C.; Yang, J.; Wang, Q.; Xiao, J.; Liao, X.; Wang, S.; Guo, Y.; Hu, W.; Liu, Y. *Adv. Mater.* **2018**, *30*, 1801951.

(20) Ni, Z.; Wang, H.; Dong, H.; Dang, Y.; Zhao, Q.; Zhang, X.; Hu, W. *Nat. Chem.* **2019**, *11*, 271−277.

(21) Yan, H.; Chen, Z.; Zheng, Y.; Newman, C.; Quinn, J. R.; Dötz, F.; Kastler, M.; Facchetti, A. *Nature* **2009**, *457*, 679−686.

(22) Picca, R. A.; Manoli, K.; Macchia, E.; Tricase, A.; Di Franco, C.; Scamarcio, G.; Cioffi, N.; Torsi, L. *Front. Chem.* **2019**, *7*, 667.

(23) Li, C.; Wu, H.; Zhang, T.; Liang, Y.; Zheng, B.; Xia, J.; Xu, J.; Miao, Q. *Chem* **2018**, *4*, 1416−1426.
(24) Hideshima, S.; Sato, R.; Kuroiwa, S.; Osaka, T. *Biosens. Bioelectron.* **2011**, *26*, 2419−2425.
(25) Buth, F.; Donner, A.; Sachsenhauser, M.; Stutzmann, M.; Garrido, J. A. *Adv. Mater.* **2012**, *24*, 4511−4517.
(26) Song, J.; Dailey, J.; Li, H.; Jang, H. J.; Zhang, P.; Wang, J. T. H.; Everett, A. D.; Katz, H. E. *Adv. Funct. Mater.* **2017**, *27*, 1606506.
(27) Shen, H.; Zou, Y.; Zang, Y.; Huang, D.; Jin, W.; Di, C. A.; Zhu, D. *Mater. Horiz.* **2018**, *5*, 240−247.
(28) Scheuermann, G. M.; Rumi, L.; Steurer, P.; Bannwarth, W.; Mülhaupt, R. *J. Am. Chem. Soc.* **2009**, *131*, 8262−8270.
(29) Zheng, L.; Li, J.; Wang, Y.; Gao, X.; Yuan, K.; Yu, X.; Ren, X.; Zhang, X.; Hu, W. *Nanoscale* **2019**, *11*, 7117−7122.
(30) Huang, Y. W.; Wu, C. S.; Chuang, C. K.; Pang, S. T.; Pan, T. M.; Yang, Y. S.; Ko, F. H. *Anal. Chem.* **2013**, *85*, 7912−7918.
(31) Magliulo, M.; Mallardi, A.; Mulla, M. Y.; Cotrone, S.; Pistillo, B. R.; Favia, P.; Vikholm-Lundin, I.; Palazzo, G.; Torsi, L. *Adv. Mater.* **2013**, *25*, 2090−2094.
(32) Suspène, C.; Piro, B.; Reisberg, S.; Pham, M. C.; Toss, H.; Berggren, M.; Yassar, A.; Horowitz, G. *J. Mater. Chem. B* **2013**, *1*, 2090−2097.
(33) Huang, J.; Miragliotta, J.; Becknell, A.; Katz, H. E. *J. Am. Chem. Soc.* **2007**, *129*, 9366−9376.
(34) Choi, H. H.; Cho, K.; Frisbie, C. D.; Sirringhaus, H.; Podzorov, V. *Nat. Mater.* **2017**, *17*, 2−7.
(35) Cheng, S.; Hotani, K.; Hideshima, S.; Kuroiwa, S.; Nakanishi, T.; Hashimoto, M.; Mori, Y.; Osaka, T. *Materials* **2014**, *7*, 2490−2500.
(36) Patel, M.; Shariff, M. I. F.; Ladep, N. G.; Thillainayagam, A. V.; Thomas, H. C.; Khan, S. A.; Taylor-Robinson, S. D. *J. Eval. Clin. Pract.* **2012**, *18*, 335−342.
(37) Zhang, L.; Wan, S.; Jiang, Y.; Wang, Y.; Fu, T.; Liu, Q.; Cao, Z.; Qiu, L.; Tan, W. *J. Am. Chem. Soc.* **2017**, *139*, 2532−2540.
(38) Galle, P. R.; Foerster, F.; Kudo, M.; Chan, S. L.; Llovet, J. M.; Qin, S.; Schelman, W. R.; Chintharlapalli, S.; Abada, P. B.; Sherman, M.; Zhu, A. X. *Liver Int.* **2019**, *39*, 2214−2229.
(39) Sun, C.; Wang, Y. X.; Sun, M.; Zou, Y.; Zhang, C.; Cheng, S.; Hu, W. *Biosens. Bioelectron.* **2020**, *164*, 112251.
(40) Qi, T.; Liao, J.; Li, Y.; Peng, J.; Li, W.; Chu, B.; Li, H.; Wei, Y.; Qian, Z. *Biosens. Bioelectron.* **2014**, *61*, 245−250.
(41) Liu, J.; Zhang, H.; Dong, H.; Meng, L.; Jiang, L.; Jiang, L.; Wang, Y.; Yu, J.; Sun, Y.; Hu, W.; Heeger, A. J. *Nat. Commun.* **2015**, *6*, 10032.
(42) Stern, E.; Wagner, R.; Sigworth, F. J.; Breaker, R.; Fahmy, T. M.; Reed, M. A. *Nano Lett.* **2007**, *7*, 3405−3409.
(43) Chua, J. H.; Chee, R. E.; Agarwal, A.; Wong, S. M.; Zhang, G.-J. *Anal. Chem.* **2009**, *81*, 6266−6271.
(44) Kaisti, M. *Biosens. Bioelectron.* **2017**, *98*, 437−448.

https://doi.org/10.1021/acs.analchem.1c00372
Anal. Chem. 2021, 93, 6188−6194